NANO LETTERS

Letter

pubs.acs.org/NanoLett

Synthetically Encoding 10 nm Morphology in Silicon Nanowires

Joseph D. Christesen,† Christopher W. Pinion,† Erik M. Grumstrup, John M. Papanikolas, and James F. Cahoon*

Department of Chemistry, University of North Carolina at Chapel Hill, Chapel Hill, North Carolina 27599-3290, United States

Supporting Information

ABSTRACT: Si nanowires (NWs) have been widely explored as a platform for photonic and electronic technologies. Here, we report a bottom-up method to break the conventional "wire" symmetry and synthetically encode a high-resolution array of arbitrary shapes, including nanorods, sinusoids, bowties, tapers, nanogaps, and gratings, along the NW growth axis. Rapid modulation of phosphorus doping combined with selective wet-chemical etching enabled morphological features as small as 10 nm to be patterned over wires more than 50 μm in length. This capability fundamentally expands the set of technologies that can be realized with Si NWs, and as proof-of-concept, we demonstrate two distinct applications. First, nanogap-encoded NWs were used as templates for Noble metals, yielding plasmonic structures with tunable resonances for surface-enhanced Raman imaging. Second, core/shell Si/SiO_2 nanorods were integrated into electronic devices that exhibit resistive switching, enabling nonvolatile memory storage. Moving beyond these initial examples, we envision this method will become a generic route to encode new functionality in semiconductor NWs.

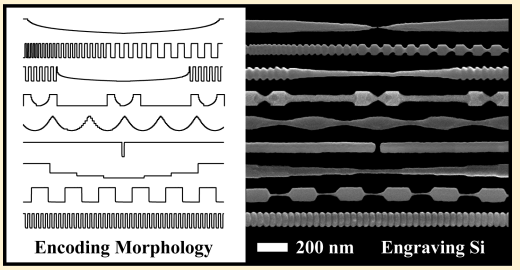

KEYWORDS: *Silicon nanowire, bottom-up lithography, plasmonics, surface-enhanced Raman spectroscopy, resistive switching*

Most semiconductor technologies rely on the ability to pattern materials with nanometer-scale features using top-down lithographic tools. Over the past decade, however, bottom-up chemical methods to control the size, shape, and composition of nanoscale materials have progressed rapidly, resulting in a diverse set of well-controlled morphologies including dots, rods, ribbons, and wires.[1−3] Semiconductor nanowires (NWs) are recognized as an especially important technological building block because the high aspect ratio can be used for longitudinal transport of electrical or optical signals.[1,2] A variety of devices have been demonstrated, including sensors,[4] waveguides,[5] phase-change memory,[6] light-emitting diodes,[7] and solar cells.[8−11] Nevertheless, current NW-based technology has been limited by the material's translational symmetry and the inability to pattern arbitrary, nanometer-scale morphological features.

NWs are typically synthesized using the vapor−liquid−solid (VLS) mechanism,[12] in which a metal nanoparticle catalyzes one-dimensional growth of a single-crystalline semiconductor material. Advancements in VLS-based technologies have generally involved synthesis of new materials or heterostructures.[13] For instance, NW superlattices, in which the composition of a NW is modulated along the growth axis, have been reported for Si/SiGe,[14] GaAs/GaP,[15] InAs/InP,[16,17] Zn-doped InP,[18] CdSe/ZnSe,[19] and P-doped Si.[20] Modulation of NW growth conditions often results in crystallographic twin planes and faceting of the NW surface, providing some capability to control morphology during synthesis.[17,18,21,22] In addition, NW superstructures have been reported in the form of controllably kinked NWs that break the one-dimensional shape.[23,24] Nevertheless, only a handful of reports describe efforts to alter the NW geometry and encode specific morphology. For example, controlled vapor−solid overcoating on the NW surface has been used to create tapered structures[25] and periodic variations in morphology.[26] In addition, modulation of the size of the metal catalyst during growth has been shown to provide control over the NW diameter.[27,28] For metal NWs, electrodeposition in metal oxide templates followed by wet-chemical etching has been used to create wires with alternating, nanoscale structures.[29,30] However, a method for accurate, nanometer-scale control of morphology in single-crystalline semiconductor NWs has not been developed. Here, we demonstrate a new method to achieve this type of high-fidelity shape control, a process which we term "ENGRAVE" for "Encoded Nanowire GRowth and Appearance through VLS and Etching." The key aspects and capabilities of this method are illustrated in Figure 1 and elaborated below.

Si NWs were grown by a VLS mechanism in a home-built, hot-wall chemical vapor deposition (CVD) system at 420 °C using Au nanoparticles as catalysts, silane (SiH_4) as the source of Si, and hydrogen (H_2) as the carrier gas (see the Supporting Information for details). As illustrated schematically in Figure 1A, an additional flow of phosphine (PH_3) was rapidly modulated during growth[20] to encode varying levels of P, an n-type substitutional dopant with high solubility in Si.[31−33] The etch rate of doped Si with aqueous KOH solution is well-known to decrease with higher dopant concentration.[34] This

Received: October 18, 2013
Revised: November 13, 2013
Published: November 25, 2013

   dx.doi.org/10.1021/nl403909r | Nano Lett. 2013, 13, 6281−6286

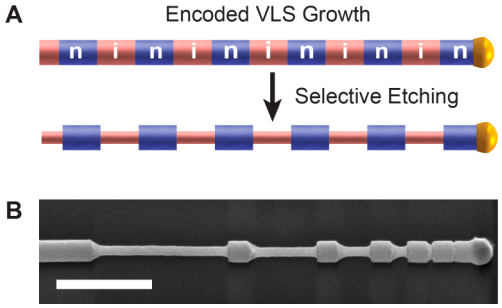

Figure 1. Synthesis of Si NWs with encoded morphology. (A) Schematic illustration of NW growth including rapid modulation of P dopant incorporation to form heavily doped n-type (n) and undoped intrinsic (i) segments that are selectively etched using wet-chemical methods to form a grating. (B) SEM image of a NW grating encoded (from left to right) with sequential intrinsic segments for 200, 100, 50, 25, 10, and 5 s; scale bar, 500 nm. Segments that are not etched correspond to an encoded n-type doping level of 5×10^{20} cm^{-3}.

effect has been observed in doped Si NWs, producing changes in diameter along the axis.[35,36] Here, we develop this effect as a tool to encode arbitrary, high-resolution morphology along the NW growth axis, enabling new technological applications of Si NWs.

To delineate the spatial resolution of the ENGRAVE process, we synthesized NWs with six intrinsic segments encoded along the axis for increasingly short time scales. As shown in Figure 1B, wet-chemical etching of these segments yielded an abrupt and conformal reduction in the NW diameter. The largest segment, encoded for 200 s, produced a feature ~700 nm in length while the smallest segment, encoded for 5 s, produced a feature ~10 nm in length, defining the lower limit of the spatial resolution for this process. This example also demonstrates that NW growth time is directly proportional to spatial length scale. Quantitative analysis of the NW growth rate yielded a value of 213 ± 6 nm/min, which was used throughout this work to convert growth times to length scales. This rate is comparatively slow because of the low CVD temperature, 420 °C, chosen to minimize radial overcoating and doping of the NW surface, a known problem during Si NW synthesis.[37,38] By minimizing the overcoating, we could encode high-fidelity nanoscale features over macroscopic length scales, as exemplified in Figure 2A by the 400 nm pitch grating encoded over 50 μm of a single NW.

For the synthesis of NWs with complex morphology, we measured the etch rate of Si NWs encoded with P doping levels ranging from 5.0×10^{20} to less than 1.0×10^{19} dopants/cm^3, as depicted in Figure 2B. Note that these doping levels were calculated from the gas-phase ratio of Si to P during CVD growth and the actual values could be lower as a result of incomplete P incorporation.[33] Quantitative evaluation of the etch rate reveals a nonlinear dependence on doping level that is well approximated with a single exponential function and varies from 2.1 nm/s for "intrinsic" segments with doping levels <1.0×10^{19} cm^{-3} to negligible etching (<0.1 nm/s) with heavily doped segments. The exponential dependence is most likely a result of the logarithmic dependence of the Fermi level position on the doping level, which modulates the rate of Si oxidation and dissolution at the semiconductor−solution interface.[34]

The precise calibration of the NW growth and etch rates enables rational design and synthesis of arbitrary high-resolution morphologies, as outlined schematically in Figure 2C. This process involves (1) design of the morphological profile, (2) conversion of the physical profile into a dopant profile, (3) VLS growth of the dopant-encoded NW, and (4) wet-chemical etching. As an example, we used this procedure to form the bowtie structure depicted in Figure 2D. The

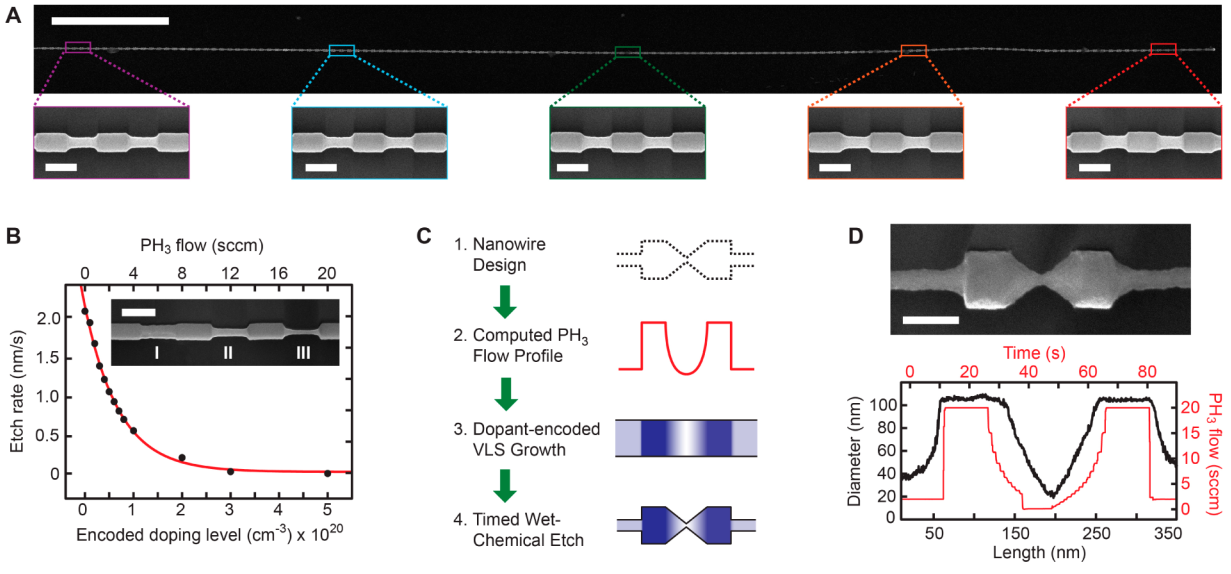

Figure 2. Characterization of NW growth, etching, and morphology. (A) Upper: SEM image of a grating-encoded NW more than 50 μm in axial length; scale bar, 5 μm. Lower: Higher-magnification SEM images of select sections of the NW in the upper panel; scale bars, 200 nm. (B) Radial etch rate of Si NWs as function of encoded P doping levels. Red curve represents the best fit to a single exponential function. Inset: SEM image of a NW with segments I, II, and III encoded with P doping levels of 1×10^{20} cm^{-3}, 5×10^{19} cm^{-3}, and intrinsic, respectively, and etched for 25 s; scale bar, 200 nm. (C) Schematic of the sequential process for bottom-up synthesis of complex NW morphologies. (D) Upper: SEM image of a NW encoded with a bowtie; scale bar, 100 nm. Lower: NW diameter (black curve and left-hand axis) as a function of length for the bowtie shown in upper panel, and measured phosphine flow rate (red curve and right-hand axis) in standard cubic centimeters per minute (sccm) as a function of time during CVD growth.

dx.doi.org/10.1021/nl403909r | Nano Lett. 2013, 13, 6281−6286

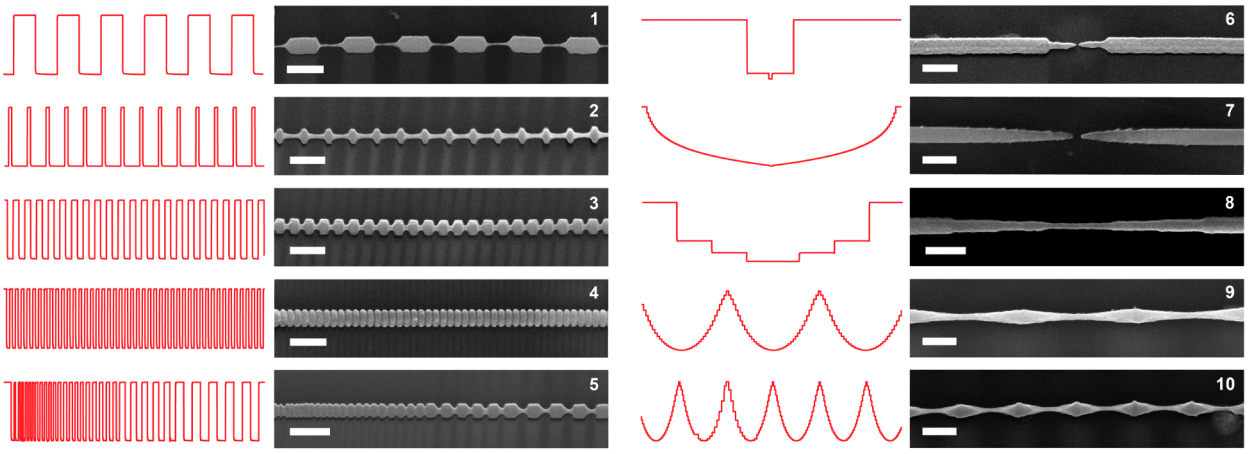

Figure 3. SEM images and phosphine flow profiles for the synthesis of Si NWs with complex morphology. The measured phosphine flow profile used to encode the morphology of each segment is depicted in red to the left of each SEM image; all scale bars, 200 nm. The flow rates vary from 0 to 20 sccm for each NW.

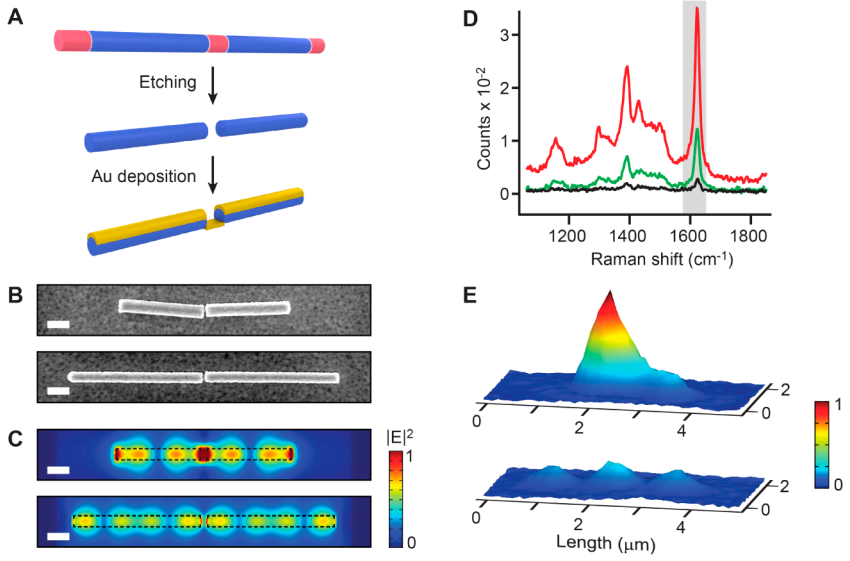

Figure 4. Nanogap-encoded NWs for plasmonics. (A) Schematic illustration of Au deposition on a nanogap-encoded NW. (B) SEM images of nanogap-encoded Si NWs with 50 nm Au, gaps of ∼30 nm, and segment lengths of ∼775 nm (upper image) and ∼1175 nm (lower image); scale bars, 200 nm. (C) Finite-element optical simulations of the Si/Au nanogap structures depicted in panel B showing the scattered field ($|E|^2$) in the plane above the NW resulting from illumination at normal incidence with a transverse-magnetic plane wave at 633 nm. The optically excited SPP mode is on-resonance and off-resonance in the upper and lower images, respectively; scale bars, 200 nm. (D) Raman spectra of methylene blue collected from the planar Au film (black), the off-resonance NW (green), and on-resonance NW (red). The shaded region denotes the spectral range used to generate spatial maps of the Raman intensity. (E) Three-dimensional spatial maps of the relative Raman signal intensity generated by raster scanning a 633 nm laser over on- and off-resonance nanogap-encoded Si/Au structures with segment lengths of ∼775 nm (upper) and ∼1175 nm (lower), respectively.

phosphine flow profile for the bowtie (red curve Figure 2D) is complex, requiring over 25 changes in flow rate over a time scale of one minute. The diameter profile (black curve Figure 2D) shows the resulting structure to be smoothly tapered with a monotonically decreasing then increasing diameter that reduces to a diameter of ∼15 nm at the narrowest point. Note that the phosphine flow profile was modified to be asymmetric around the flow minimum to account for dopants retained by the Au catalyst, a phenomenon termed the reservoir effect.[39]

We used other complex doping profiles to encode the range of morphological features shown in SEM images in Figure 3. These structures include periodic (images 1−4) or nonperiodic (image 5) gratings, nanogaps with gap sizes as small as 10 nm (images 6−7), suspended nanorods (image 8), and sinusoidal profiles (images 9−10). These morphologies could each enable a different class of NW-based technology. For instance, the suspended nanorods could be used as mechanical oscillators for nanoelectromechanical systems,[40] periodic gratings for optical applications in nanophotonics,[41] and nonperiodic gratings as a method to control thermal transport along the wires, enabling the use of Si as a thermoelectric material.[42,43] Although full development of these applications is outside the scope of this work, below we highlight two distinct applications of ENGRAVE NWs in the areas of plasmonics (Figure 4) and electronics (Figure 5).

Field-enhanced spectroscopies, such as surface-enhanced Raman spectroscopy (SERS), are often performed using Noble metal nanostructures that support surface plasmon

dx.doi.org/10.1021/nl403909r | Nano Lett. 2013, 13, 6281−6286

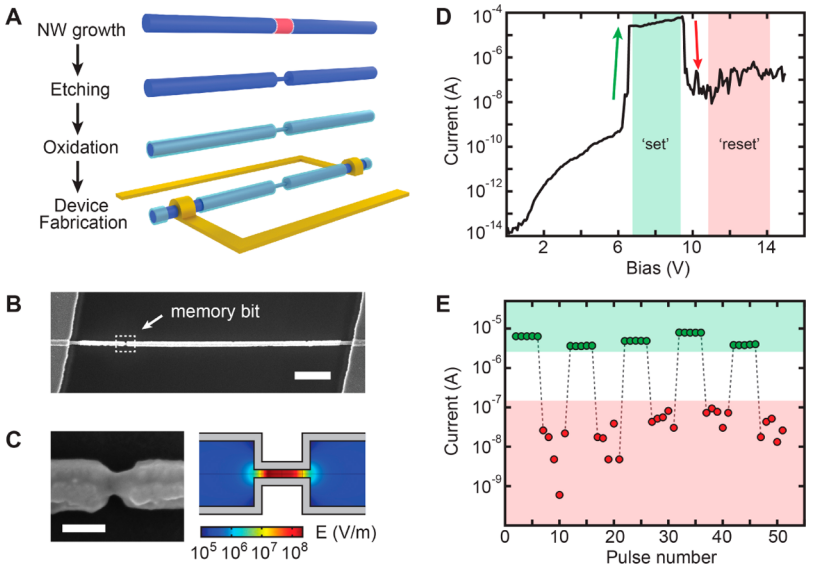

Figure 5. Nanorod-encoded NWs for nonvolatile memory. (A) Schematic illustration of the sequential process used to fabricate a nonvolatile memory bit. (B) SEM image of a NW device encoded with a nonvolatile memory bit (dashed box) showing Ti/Pd Ohmic contacts on the far left and right; scale bar, 1 μm. (C) Left: SEM image of the encoded memory bit corresponding to the dashed white box in panel B; scale bar, 100 nm. Right: finite-element simulation of the electric field magnitude across the NW at an applied bias of +8 V plotted in a logarithmic color scale for a nanorod segment 50 nm in length and 10 nm in diameter. (D) Characteristic switching $I-V$ curve for an ENGRAVE NW memory device. The shaded green and red regions define the set and reset bias ranges, respectively. (E) Resistive switching behavior over 10 memory cycles. Dashed lines represent the set/reset pulses between current readings, which were acquired five times at 1 V between each set or reset pulse.

polaritons (SPPs).[44] Through careful design of the shape of a nanostructure, SPP resonances can be used to confine and amplify incident electromagnetic fields at specific wavelengths and spatial positions.[45] Following the procedure depicted in Figure 4A, we used nanogap-encoded NWs as the topological templates for Noble metal films, creating Si/Au nanostructures with tunable SPP resonances. As shown by the SEM images in Figure 4B, deposition of ~50 nm of Au on the NWs by physical vapor deposition preserved the high-resolution structures and nanogap morphology. We used finite-element optical simulations (see Figure 4C) to design Si/Au ENGRAVE structures with specific SPP characteristics. The NWs behave as plasmonic resonator antennas[46] in which the length of the segments adjacent to the gap control the field enhancement as a result of constructive or destructive interference of the SPP wave along the NW axis.[47,48] For a wavelength of 633 nm, we found that segments ~775 nm in length were on-resonance, producing intense fields in the gap, while segments ~1175 nm in length were off-resonance, exhibiting weaker field enhancement. As proof-of-concept, we performed SERS imaging on the Si/Au NWs coated with methylene blue.[47,48] We observed a greater than 10-fold Raman signal enhancement from the on-resonance structure, as shown by the spectra in Figure 4D. In addition, Raman imaging (see Figure 4E) confirmed that the signal enhancement is localized to a narrow spatial region around the gap. In comparison, the off-resonance NW shows a weak Raman signal arising from both the gap and the two ends of the rods, a result that is in good agreement with the optical simulations in Figure 4C. These results highlight the capability for ENGRAVE to serve as a simple route to create nanoplasmonic structures with tunable resonances for field-enhanced spectroscopy[44] and nanophotonic technologies.[45]

As a second application of ENGRAVE, we fabricated core/shell Si/SiO_2 nanorod-encoded devices for use as resistive switches in nonvolatile memory.[6,49,50] The fabrication steps are illustrated in Figure 5A. First, an n-type/intrinsic/n-type NW was synthesized with a 50 nm intrinsic channel. Second, the channel was etched to a diameter of ~30 nm to produce a suspended nanorod. Third, the wire was thermally oxidized to create a ~10 nm diameter Si core encased by an oxide shell. Fourth, electrical contacts were fabricated to the two n-type segments adjacent to the intrinsic channel, as shown by the SEM image in Figure 5B. Device simulations[51] (see Figure 5C) indicate that this geometry concentrates the voltage drop and electric field within the narrow channel region, enabling a resistive switching effect as observed in a planar Si/SiO_2 system.[49,50] Initial current–voltage ($I-V$) measurements showed an Ohmic response from the device with a resistance of 54.7 kΩ, indicating the presence of a thin Si filament encapsulated by the SiO_2 shell. After an electroforming process consisting of multiple $I-V$ sweeps at high bias (see the Supporting Information for details), the device converged to the characteristic "switching" $I-V$ behavior (see Figure 5D) expected from a Si/SiO_2 system.[49,50] The $I-V$ curve exhibits a low voltage region that "sets" the device to a low resistance state and a high voltage region that "resets" the device to a high resistance state. In the latter state, we observed variations in the current (see Figure 5D,E) similar to those reported previously in Si/SiO_2 resistive switching memory devices and attributed to tunneling current fluctuations.[49]

To use the nanorod-encoded device as nonvolatile memory, we applied sequential "set" and "reset" voltage pulses (100 μs) of 8 and 12 V, respectively, to reversibly change the resistance of the device. As shown in Figure 5E, we cycled the NW device through ten memory states and achieved on/off current ratios of nearly 10^2. With further development, we expect that at least 100 memory bits could be encoded on a single NW and lower voltage operation achieved with smaller nanorod segments. These initial results demonstrate the facile integration of ENGRAVE structures in electronic devices and furthermore

dx.doi.org/10.1021/nl403909r | *Nano Lett.* 2013, 13, 6281–6286

highlight the emergent electronic characteristics that can be encoded through morphology.

In summary, we have demonstrated a method, termed ENGRAVE, to encode high-resolution morphology along the growth axis of Si NWs. We anticipate this process will be extended to other NW materials, such as GaAs/GaP[52,53] et al., that can be selectively etched with gas-phase or wet-chemical techniques and will represent a general route to encode new functionality in semiconductor NWs.

■ ASSOCIATED CONTENT

Supporting Information

Details of NW synthesis, characterization methods, device fabrication, and measurements. This material is available free of charge via the Internet at http://pubs.acs.org.

■ AUTHOR INFORMATION

Corresponding Author

*E-mail: jfcahoon@unc.edu.

Author Contributions

†J.D.C. and C.W.P. contributed equally.

Notes

The authors declare no competing financial interest.

■ ACKNOWLEDGMENTS

J.D.C., C.W.P., and J.F.C. acknowledge support from the National Science Foundation through Grant DMR-1308695, and E.M.G. and J.M.P acknowledge support through Grant CHE-1213379. We thank T. Celano, C. Flynn, and X. Zhang for useful discussions and help with figure preparation and S. Sheiko for comments on the manuscript. We also thank the staff of the Chapel Hill Analytical and Nanofabrication Laboratory (CHANL) user facility for assistance with NW imaging and K. Brennaman for assistance with Raman imaging.

■ REFERENCES

(1) Lieber, C. M. *MRS Bull.* **2011**, *36*, 1052.
(2) Yang, P.; Yan, R.; Fardy, M. *Nano Lett.* **2010**, *10*, 1529.
(3) Choi, C. L.; Alivisatos, A. P. From artificial atoms to nanocrystal molecules: Preparation and properties of more complex nanostructures. *Annu. Rev. Phys. Chem.* **2010**, *61*, 369−389.
(4) Cui, Y.; Wei, Q.; Park, H.; Lieber, C. M. *Science* **2001**, *293*, 1289.
(5) Law, M.; Sirbuly, D. J.; Johnson, J. C.; Goldberger, J.; Saykally, R. J.; Yang, P. D. *Science* **2004**, *305*, 1269.
(6) Lee, S.-H.; Jung, Y.; Agarwal, R. *Nat. Nanotechnol.* **2007**, *2*, 626.
(7) Qian, F.; Li, Y.; Gradečak, S.; Wang, D.; Barrelet, C. J.; Lieber, C. M. *Nano Lett.* **2004**, *4*, 1975.
(8) Tian, B.; Kempa, T. J.; Lieber, C. M. *Chem. Soc. Rev.* **2009**, *38*, 16.
(9) Kempa, T. J.; Day, R. W.; Kim, S.-K.; Park, H.-G.; Lieber, C. M. *Energy Environ. Sci.* **2013**, *6*, 719.
(10) Zhang, X.; Pinion, C. W.; Christesen, J. D.; Flynn, C. J.; Celano, T. A.; Cahoon, J. F. *J. Phys. Chem. Lett.* **2013**, *4*, 2002.
(11) Hochbaum, A. I.; Yang, P. D. *Chem. Rev.* **2010**, *110*, 527.
(12) Wagner, R. S.; Ellis, W. C. *Appl. Phys. Lett.* **1964**, *4*, 89.
(13) Li, Y.; Qian, F.; Xiang, J.; Lieber, C. M. *Mater. Today.* **2006**, *9*, 18.
(14) Wu, Y. Y.; Fan, R.; Yang, P. D. *Nano Lett.* **2002**, *2*, 83.
(15) Gudiksen, M. S.; Lauhon, L. J.; Wang, J.; Smith, D. C.; Lieber, C. M. *Nature* **2002**, *415*, 617.
(16) Bjork, M. T.; Ohlsson, B. J.; Sass, T.; Persson, A. I.; Thelander, C.; Magnusson, M. H.; Deppert, K.; Wallenberg, L. R.; Samuelson, L. *Nano Lett.* **2002**, *2*, 87.
(17) Eymery, J.; Rieutord, F.; Favre-Nicolin, V.; Robach, O.; Niquet, Y. M.; Froberg, L.; Martensson, T.; Samuelson, L. *Nano Lett.* **2007**, *7*, 2596.
(18) Algra, R. E.; Verheijen, M. A.; Borgstrom, M. T.; Feiner, L.-F.; Immink, G.; van Enckevort, W. J. P.; Vlieg, E.; Bakkers, E. P. A. M. *Nature* **2008**, *456*, 369.
(19) Laocharoensuk, R.; Palaniappan, K.; Smith, N. A.; Dickerson, R. M.; Werder, D. J.; Baldwin, J. K.; Hollingsworth, J. A. *Nat. Nanotechnol.* **2013**, *8*, 660.
(20) Yang, C.; Zhong, Z.; Lieber, C. M. *Science* **2005**, *310*, 1304.
(21) Ross, F. M.; Tersoff, J.; Reuter, M. C. *Phys. Rev. Lett.* **2005**, *95*, 146104.
(22) Caroff, P.; Dick, K. A.; Johansson, J.; Messing, M. E.; Deppert, K.; Samuelson, L. *Nat. Nanotechnol.* **2009**, *4*, 50.
(23) Lilach, Y.; Zhang, J. P.; Moskovits, M.; Kolmakov, A. *Nano Lett.* **2005**, *5*, 2019.
(24) Tian, B.; Xie, P.; Kempa, T. J.; Bell, D. C.; Lieber, C. M. *Nat. Nanotechnol.* **2009**, *4*, 824.
(25) Chueh, Y. L.; Fan, Z. Y.; Takei, K.; Ko, H.; Kapadia, R.; Rathore, A. A.; Miller, N.; Yu, K.; Wu, M.; Haller, E. E.; Javey, A. *Nano Lett.* **2010**, *10*, 520.
(26) Musin, I. R.; Boyuk, D. S.; Filler, M. A. *J. Vac. Sci. Technol., B* **2013**, *31*, 020603.
(27) Lim, S. K.; Crawford, S.; Haberfehlner, G.; Gradečak, S. *Nano Lett.* **2013**, *13*, 331.
(28) Crawford, S.; Lim, S. K.; Gradečak, S. *Nano Lett.* **2013**, *13*, 226.
(29) Kline, T. R.; Tian, M. L.; Wang, J. G.; Sen, A.; Chan, M. W. H.; Mallouk, T. E. *Inorg. Chem.* **2006**, *45*, 7555.
(30) Qin, L. D.; Park, S.; Huang, L.; Mirkin, C. A. *Science* **2005**, *309*, 113.
(31) Zheng, G. F.; Lu, W.; Jin, S.; Lieber, C. M. *Adv. Mater.* **2004**, *16*, 1890.
(32) Wang, Y. F.; Lew, K. K.; Ho, T. T.; Pan, L.; Novak, S. W.; Dickey, E. C.; Redwing, J. M.; Mayer, T. S. *Nano Lett.* **2005**, *5*, 2139.
(33) Schmid, H.; Bjork, M. T.; Knoch, J.; Karg, S.; Riel, H.; Riess, W. *Nano Lett.* **2009**, *9*, 173.
(34) Seidel, H.; Csepregi, L.; Heuberger, A.; Baumgartel, H. *J. Electrochem. Soc.* **1990**, *137*, 3626.
(35) Kempa, T. J.; Tian, B.; Kim, D. R.; Hu, J.; Zheng, X.; Lieber, C. M. *Nano Lett.* **2008**, *8*, 3456.
(36) Cohen-Karni, T.; Casanova, D.; Cahoon, J. F.; Qing, Q.; Bell, D. C.; Lieber, C. M. *Nano Lett.* **2012**, *12*, 2639.
(37) Perea, D. E.; Hemesath, E. R.; Schwalbach, E. J.; Lensch-Falk, J. L.; Voorhees, P. W.; Lauhon, L. J. *Nat. Nanotechnol* **2009**, *4*, 315.
(38) Schmid, H.; Bjork, M. T.; Knoch, J.; Riel, H.; Riess, W.; Rice, P.; Topuria, T. *J. Appl. Phys.* **2008**, *103*, 024304.
(39) Wen, C. Y.; Reuter, M. C.; Bruley, J.; Tersoff, J.; Kodambaka, S.; Stach, E. A.; Ross, F. M. *Science* **2009**, *326*, 1247.
(40) He, R. R.; Feng, X. L.; Roukes, M. L.; Yang, P. D. *Nano Lett.* **2008**, *8*, 1756.
(41) Lindquist, N. C.; Nagpal, P.; McPeak, K. M.; Norris, D. J.; Oh, S. H. *Rep. Prog. Phys.* **2012**, *75*, 036501.
(42) Hochbaum, A. I.; Chen, R.; Delgado, R. D.; Liang, W.; Garnett, E. C.; Najarian, M.; Majumdar, A.; Yang, P. *Nature* **2008**, *451*, 163.
(43) Zianni, X. *Appl. Phys. Lett.* **2010**, *97*, 233106.
(44) Willets, K. A.; Van Duyne, R. P. Localized surface plasmon resonance spectroscopy and sensing. *Annu. Rev. Phys. Chem.* **2007**, *58*, 267.
(45) Schuller, J. A.; Barnard, E. S.; Cai, W.; Jun, Y. C.; White, J. S.; Brongersma, M. L. *Nat. Mater.* **2010**, *9*, 193.
(46) Barnard, E. S.; White, J. S.; Chandran, A.; Brongersma, M. L. *Opt. Express.* **2008**, *16*, 16529.
(47) Pedano, M. L.; Li, S. Z.; Schatz, G. C.; Mirkin, C. A. *Angew. Chem., Int. Ed.* **2010**, *49*, 78.
(48) Li, S. Z.; Pedano, M. L.; Chang, S. H.; Mirkin, C. A.; Schatz, G. C. *Nano Lett.* **2010**, *10*, 1722.
(49) Yao, J.; Sun, Z.; Zhong, L.; Natelson, D.; Tour, J. M. *Nano Lett.* **2010**, *10*, 4105.
(50) Yao, J.; Zhong, L.; Natelson, D.; Tour, J. M. *Sci. Rep.* **2012**, *2*, 242.
(51) Christesen, J. D.; Zhang, X.; Pinion, C. W.; Celano, T. A.; Flynn, C. J.; Cahoon, J. F. *Nano Lett.* **2012**, *12*, 6024.

(52) Kallesoe, C.; Molhave, K.; Martensson, T.; Hansen, T. M.; Samuelson, L.; Boggild, P. *Microelectron. Eng.* **2008**, *85*, 1179.
(53) Kallesoe, C.; Molhave, K.; Larsen, K. F.; Engstrom, D.; Hansen, T. M.; Boggild, P.; Martensson, T.; Borgstrom, M.; Samuelson, L. *J. Vac. Sci. Technol., B* **2010**, *28*, 21.